Research Square

Preprints are preliminary reports that have not undergone peer review.
They should not be considered conclusive, used to inform clinical practice,
or referenced by the media as validated information.

Leading-Edge Turbulence Intensity as a Compact Descriptor of Laminar Separation over a NACA 0012 Airfoil

Montaser Saeed

montaser.saeed@bsu.edu.ly

Bright Star University

Alnazir Alatta

Karary University

Saad Adam

Tobruk University

Abdelgader Agilah

Bright Star University

Research Article

Keywords: Laminar separation bubble, Transition SST, Freestream turbulence, Turbulence length scale, NACA 0012, Low-Reynolds-number aerodynamics

Posted Date: October 8th, 2026

DOI: https://doi.org/10.21203/rs.3.rs-11197109/v1

License: This work is licensed under a Creative Commons Attribution 4.0 International License.
Read Full License

Additional Declarations: No competing interests reported.

Leading-Edge Turbulence Intensity as a Compact Descriptor of Laminar Separation over a NACA 0012 Airfoil

Montaser Saeed[1], *, Alnazir Alatta[2], Saad Adam[3], Abdelgader Agilah[4]

[1] Department of Aeronautical Engineering, Bright Star University, El Brega, Libya
[2] Department of Aeronautical Engineering, Faculty of Engineering, Karary University, Khartoum, Sudan
[3] Department of Mechanical Engineering, Faculty of Engineering, Tobruk University, Tobruk, Libya
[4] Department of Mechanical Engineering, Faculty of Technical Engineering, Bright Star University, El Brega, Libya

*Corresponding author: montaser.saeed@bsu.edu.ly

Abstract

Freestream turbulence intensity and turbulence length scale jointly influence transitional separation over low-Reynolds-number airfoils, yet their combined effect is often characterized using nominal inlet conditions. This study examines whether the turbulence intensity reaching the leading-edge region provides a more compact descriptor of the predicted separation response. Two-dimensional steady Reynolds-averaged Navier–Stokes (RANS) simulations were performed for a NACA 0012 airfoil at $Re_c = 1.0 \times 10^5$using the correlation-based Transition Shear Stress Transport (Transition SST) model. The 105-case matrix covered seven angles of attack, five nominal freestream turbulence intensities (Tu_∞ = 0.15–4%), and three inlet turbulence length scales (L_s = 0.01–0.10 m). A reference-normalized leading-edge turbulence intensity (Tu_{LE}) was extracted from the computed upstream field, while separation (x_s) and reattachment (x_r) were identified from signed skin friction. At fixed Tu_∞, varying $L_s$produced appreciable differences in Tu_{LE}. Reparameterization using Tu_{le} reduced out-of-group prediction errors for x_s by approximately 49–61% at α = 0°, ±2°, and ±4°, with positive gains across all tested statistical models. Reattachment showed statistically supported reductions of approximately 50% and 81% at ±4° and 6°, respectively, whereas the ±2° comparison was inconclusive. Adding L_s after Tu_{LE} provided no additional cross-validated predictive benefit. Comparison with high-fidelity reference results recovered the mean closed-bubble topology. Within the investigated framework and parameter space, $Tu_{LE\ e}$ provides a more compact descriptor of predicted laminar-separation response than nominal Tu_∞.

Keywords: Laminar separation bubble; Transition SST; Freestream turbulence; Turbulence length scale; NACA 0012; Low-Reynolds-number aerodynamics

1. Introduction

Low-Reynolds-number airfoils exhibit strong coupling among laminar separation, transition, and turbulent reattachment, with direct consequences for small uncrewed aerial vehicles, micro-air vehicles, and compact wind-energy systems (Lissaman 1983; Mueller and DeLaurier 2003). Under an adverse pressure gradient, a laminar boundary layer may separate before transition. Disturbances subsequently amplify in the detached shear layer and, if transition provides sufficient momentum exchange, the flow can reattach to form a laminar separation bubble (LSB) (Tani 1964; Gaster 1967; O'Meara and Mueller 1987; Boutilier and Yarusevych 2012a). Changes in this sequence modify surface pressure and skin friction and can produce nonlinear variations in lift, drag, hysteresis, and stall behavior (O'Meara and Mueller 1987; Boutilier and Yarusevych 2012a; Hain et al. 2009; Jardin et al. 2025). Such sensitivity becomes particularly important at low Reynolds numbers, where modest changes in the disturbance environment can alter the separated-flow topology. Freestream turbulence is a major component of this environment. Experiments have shown that increasing turbulence intensity generally advances transition and reattachment and reduces LSB extent (Istvan et al. 2018; Istvan and Yarusevych 2018). High-fidelity simulations further indicate that the transition pathway changes with disturbance level, as modal shear-layer amplification increasingly interacts with streak-like and non-modal mechanisms (Balzer and Fasel 2016; Hosseinverdi and Fasel 2019). Studies of the NACA 0012 similarly report substantial changes in surface-flow topology and aerodynamic loading with freestream turbulence (Wang et al. 2014; Huang and Lee 1999; Hrynuk et al. 2024; Yu et al. 2024). Although these investigations consistently establish turbulence intensity as an important parameter, they also show that the response depends on how disturbances evolve before and after separation. A nominal upstream intensity therefore does not fully characterize the disturbance environment the boundary layer encounters. Turbulence scale introduces a physically distinct influence, although its importance relative to disturbance amplitude remains case dependent.

Disturbances of comparable intensity but different characteristic scales can interact differently with the attached boundary layer and separated shear layer. Scale sensitivity is established in bypass transition (Jonáš et al. 2000), and airfoil studies have reported changes in receptivity, transition development, and LSB characteristics when the integral or imposed turbulence scale is varied (Jaroslawski et al. 2023; Breuer 2018; Kawai et al. 2023; Thompson et al. 2023; Toppings and Yarusevych 2025). The reported effects are not uniform. Jaroslawski et al. (2023), for example, observed scale-dependent changes in disturbance development, while the mean bubble remained more strongly influenced by turbulence intensity; scale-resolved computations have reported appreciable sensitivity to both quantities (Breuer 2018; Kawai et al. 2023). Studies involving energetic large-scale disturbances provide further evidence that scale can modify separated-flow organization (Thompson et al. 2023; Toppings and Yarusevych 2025). Taken together, these results establish scale sensitivity without implying that its contribution to the mean LSB response is independent of, or comparable in magnitude to, that of turbulence intensity. In a RANS transition calculation, however, this physical sensitivity must first be distinguished from the effect of transporting the prescribed inlet turbulence toward the airfoil. Turbulence quantities imposed at a remote inlet evolve before reaching the leading-edge region. Consequently, cases with the same nominal freestream turbulence intensity, Tu_∞, but different prescribed inlet turbulence length scales, L_s, need not deliver the same turbulence state to the airfoil. This issue is directly relevant to the correlation-based Transition Shear Stress Transport (Transition SST) model developed through the local-correlation framework of Menter et al. (2006) and the subsequent $\gamma - Re_\theta$ formulation of Langtry and Menter (2009). The transition correlations

depend on locally evaluated quantities coupled to the transported turbulence field. In particular, local turbulence intensity is related to turbulent kinetic energy through $Tu = 100\sqrt{2k/3}/U$. Thus, changes in the upstream evolution of k alter the turbulence level presented to the transition model even when Tu_∞ is unchanged. This modeling consideration defines the specific question addressed here. Previous studies establish that freestream turbulence influences separation-induced transition (Huang and Lee 1999; Wang et al. 2014; Balzer and Fasel 2016; Istvan et al. 2018; Istvan and Yarusevych 2018; Hosseinverdi and Fasel 2019; Hrynuk et al. 2024; Yu et al. 2024), that disturbance scale can affect boundary-layer and separated-shear-layer development (Jonáš et al. 2000; Breuer 2018; Kawai et al. 2023; Jaroslawski et al. 2023; Thompson et al. 2023; Toppings and Yarusevych 2025), and that Transition SST responds to turbulence quantities that evolve locally (Menter et al. 2006; Langtry and Menter 2009). However, it remains unclear whether the apparent dependence of Transition SST separation predictions on Tu_∞ and prescribed L_s can be reorganized using the turbulence intensity actually delivered to the leading-edge region. An observed L_s dependence may partly reflect upstream evolution of the modeled turbulence rather than an independent contribution to the predicted aerodynamic response. Distinguishing these effects is necessary before assigning physical significance to inlet-length-scale sensitivity in parametric RANS calculations. This study examines that question for a NACA 0012 airfoil at a chord Reynolds number of $Re_c = 1.0 \times 10^5$. A full-factorial database of 105 two-dimensional, steady RANS simulations combines seven angles of attack, five nominal turbulence intensities ($Tu_\infty = 0.15$–4%), and three prescribed inlet turbulence length scales ($L_s = 0.01$–0.10 m). The computed upstream turbulence field is used to determine the leading-edge turbulence intensity, Tu_{LE}, independently of the resulting separation location. We identify separation and reattachment from the signed skin-friction coefficient. Symmetry-based numerical checks and grouped cross-validation then assess whether relationships obtained across different inlet specifications remain reproducible. The testable hypothesis is that Tu_{LE} provides a more compact representation of the predicted separation response than Tu_∞, as measured by out-of-group predictive error. A successful reparameterization should reduce the systematic dependence on L_s; any residual predictive contribution from L_s would indicate that Tu_{LE} alone does not capture the full modeled response. This work therefore quantifies the separation of these two effects rather than assuming that turbulence-scale sensitivity disappears. The conclusions are restricted to the investigated Transition SST framework and parameter space and do not imply that physical length-scale effects are reducible to local turbulence intensity. From an engineering-modeling perspective, the analysis tests whether transition-sensitive RANS studies should report leading-edge turbulence conditions rather than nominal inlet values alone.

2. Computational Methodology

2.1. Numerical framework and transition modelling

Flow over the NACA 0012 airfoil was simulated using the finite-volume method implemented in **ANSYS Fluent 2024 R1**. Two-dimensional, double-precision, pressure-based steady Reynolds-averaged Navier-Stokes (RANS) calculations were conducted. The computational approach systematically examined how separation topology, as predicted by a fixed transition-modelling framework, responds to the turbulence state delivered to the leading-edge region. These calculations were not intended to resolve the instantaneous three-dimensional dynamics of a laminar separation bubble (LSB). The chord Reynolds number was fixed at

$$Re_c = \frac{\rho U_\infty c}{\mu} = 1.0 \times 10^5, \qquad (1)$$

where $\rho = 1.225\ \mathrm{kg\,m^{-3}}$ and $\mu = 1.7894 \times 10^{-5}\ \mathrm{kg\,m^{-1}\,s^{-1}}$, giving $U_\infty = 1.461\ \mathrm{m\,s^{-1}}$. These quantities were held constant throughout the computational matrix. Transition was represented using the correlation-based Transition Shear Stress Transport (Transition SST) model, also referred to as the $\gamma - Re_\theta$ formulation. The model augments the SST turbulence closure with transport equations for intermittency and a transition-onset momentum-thickness Reynolds-number variable. The complete transport equations, empirical correlations, and model constants are provided by Menter et al. (2006) and Langtry and Menter (2009) and are therefore not reproduced here. The standard ANSYS Fluent implementation was retained without case-specific recalibration. Accordingly, the study examines the response of a fixed transition model to changes in prescribed inlet turbulence conditions rather than tuning its correlations to individual cases. At the inlet, the nominal freestream turbulence intensity, Tu_∞, determines the turbulent kinetic energy according to

$$k_\infty = \frac{3}{2}\left(U_\infty \frac{Tu_\infty}{100}\right)^2. \qquad (2)$$

The prescribed turbulence length-scale parameter, L_s, supplies the corresponding scale information required by the turbulence boundary condition. Throughout this paper, L_s refers specifically to the inlet turbulence length-scale parameter used by the computational model. It is not equated with the physical integral length scale experienced locally by the boundary layer or separated shear layer. This distinction is central to the analysis because different combinations of Tu_∞ and L_s may produce different upstream evolutions of turbulent kinetic energy before the flow reaches the airfoil. Nominal inlet intensity therefore does not represent the turbulence state encountered near the leading edge.

2.2. Computational domain and boundary conditions

Figure 1 presents the computational domain and mesh topology. The domain extends approximately 14c upstream of the leading edge, 25c downstream of the trailing edge, and 15c above and below the chord line. These extents were chosen to limit direct boundary interference while allowing the prescribed turbulence field to evolve over a finite upstream distance. The NACA 0012 geometry remained fixed throughout the simulations, and the angle of attack was imposed by rotating the incoming velocity vector rather than the airfoil. A velocity-inlet condition was applied at the upstream boundary, and the downstream boundary was specified as a pressure outlet. The airfoil surface was treated as a stationary no-slip wall. The freestream velocity magnitude and fluid properties were held constant throughout the computational matrix, with only the prescribed incidence and turbulence conditions varied according to the test matrix. Pressure–velocity coupling was handled using the Semi-Implicit Method for Pressure-Linked Equations-Consistent (SIMPLEC) algorithm, with second-order spatial discretization. The same solver formulation, computational domain, and numerical settings were maintained across all cases to avoid configuration-dependent variability in the parametric comparisons.

2.3. Full-factorial computational design

The parameter space was constructed as a full-factorial design comprising seven angles of attack,

$$\alpha = [-4°, -2°, 0°, 2°, 4°, 6°, 8°] \qquad (3)$$

five nominal freestream turbulence intensities,

$$Tu_\infty = [0.15, 0.5, 1, 2, 4]\%, \qquad (4)$$

and three prescribed inlet turbulence length scales,

$$\frac{L_s}{c} = [0.01, 0.05, 0.1]. \qquad (5)$$

The complete matrix therefore contained

$$7 \times 5 \times 3 = 105$$

steady Transition SST calculations. The factorial design allows Tu_∞ and L_s to be varied independently rather than through a one-factor-at-a-time sequence.

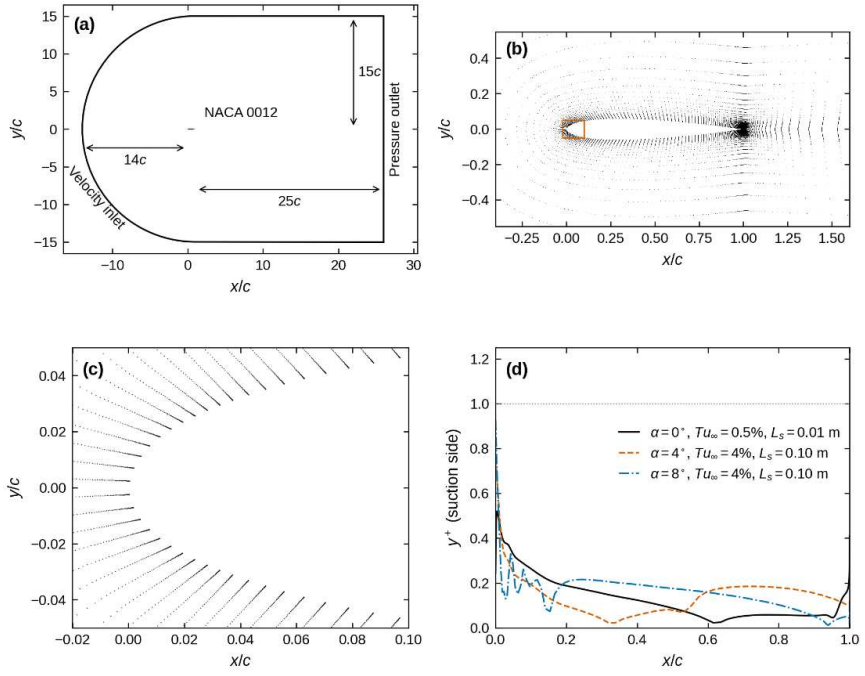


Fig. 1. Computational domain, mesh topology, and near-wall resolution: (a) computational domain and boundary locations normalized by the airfoil chord; (b) mesh distribution around the NACA 0012 airfoil and downstream wake; (c) enlarged view of the leading-edge mesh; and (d) suction-side wall-coordinate distribution for representative operating conditions. The dotted horizontal line denotes y^+=1.

These mirrored conditions were subsequently used as an internal numerical-consistency diagnostic. They were not treated as experimental validation. Their apparent joint influence can consequently be examined before and after accounting for the turbulence intensity actually delivered to the leading-edge region. The geometric symmetry of the NACA 0012 also provides corresponding positive- and negative-incidence cases at $\alpha = 2°$and $4°$.

2.4. Mesh resolution and near-wall treatment

Three successively refined structured quadrilateral meshes were used to assess sensitivity to spatial resolution, with refinement concentrated around the airfoil and extending through the near-wall, separated-flow, and wake regions [Fig. 1(b,c)]. The Coarse, Medium, and Fine meshes contained 10,019, 22,780, and 40,859 cells, respectively, with 129, 167, and 249 airfoil-surface sampling points (Table 1). The same structured topology was retained across the three refinement levels. Based on this assessment, the fine mesh was adopted for all 105 production calculations. Further structured refinement was not pursued because simultaneous refinement of the near-wall and wake regions rapidly increases computational and memory requirements.

Table 1. Characteristics of the structured meshes used in the grid-sensitivity assessment.

Grid	Cells	Nodes	Airfoil-surface samples
Coarse	10,019	10,243	129
Medium	22,780	23,099	167
Fine	40,859	41,299	249

The Fine-grid solution fields contained 41,299 computational nodes, including the same 249 airfoil-wall nodes in every case. Near-wall resolution was assessed directly from the computed y^+distribution because both the Transition SST formulation and the signed-wall-shear identification of separation and reattachment require adequate resolution of the viscous near-wall region. Across the 105 calculations, the maximum y^+remained below unity, while the median of the case-wise maxima was approximately 0.75. Representative suction-side distributions are shown in Fig. 1(d). We retained the same Fine mesh and numerical settings throughout the factorial database, preventing spatial discretization from becoming an additional varying factor among cases. We examined residual histories and aerodynamic-force monitors together to assess numerical stabilization. A residual target of 10^{-5} was used, supplemented by the late-iteration behaviour of the aerodynamic coefficients. Some transitional cases retained small late-iteration fluctuations rather than reaching a strictly invariant numerical state. The reported quantities are therefore interpreted as stabilized steady Transition SST predictions rather than evidence of physically steady flow.

2.5. Leading-edge turbulence descriptor and separation extraction

The leading-edge turbulence intensity characterized the turbulence state approaching the airfoil, Tu_{LE}, evaluated at a point located $0.35c$ upstream of the leading edge along the incoming-flow direction,

$$x_{LE}^{*} = -0.35c(\cos\alpha\,, \sin\alpha). \qquad (7)$$

The turbulent kinetic energy at this location was obtained by linear interpolation of the exported solution field using a Delaunay triangulation constructed from computational nodes within $1.5c$of the leading edge. The turbulence descriptor was then reconstructed directly from the interpolated turbulent kinetic energy,

$$Tu_{LE} = 100\frac{\sqrt{2k_{LE}/3}}{U_\infty}. \qquad (8)$$

The common reference velocity $U_\infty = 1.461\ \mathrm{m\ s^{-1}}$was used instead of the local velocity so that variations in Tu_{LE}primarily reflected the upstream evolution of turbulent kinetic energy rather than local acceleration effects. As a consistency check, $0.961 \le U_{\mathrm{loc}}/U_\infty \le 0.972$across the sampled cases; replacing $U_\infty$with U_{loc}changed the reconstructed descriptor by only approximately 3–4% without altering the ordering of cases. Furthermore, shifting the sampling station to $0.25c$or $0.50c$upstream changed $Tu_{LE}$by less than 0.6%, whereas the maximum incidence-dependent variation for a fixed $(T, u_\infty L_s)$ combination was approximately 0.9%. Consequently, Tu_{LE} was evaluated independently upstream of the subsequently determined separation response; conceptually, the analysis examines the progression from $(T, u_\infty L_s)$to Tu_{LE} and finally to the predicted separation behaviour. Separation and reattachment locations were extracted from the signed tangential wall shear rather than the unsigned skin-friction magnitude exported directly by Fluent. We divided the 249 wall nodes into upper and lower surfaces and ordered them chordwise. Using the local unit tangent vector $t = (t_x, t_y)$, the signed wall shear and corresponding skin-friction coefficient were computed as

$$\tau_{w,t} = \tau_{w,x}t_x + \tau_{w,y}t_y. \qquad (9)$$

$$C_f = \frac{\tau_{w,t}}{\frac{1}{2}\rho U_\infty^2}. \qquad (10)$$

A positive-to-negative $C_f$crossing defined the separation location, x_s, while the subsequent negative-to-positive crossing defined a candidate reattachment location, x_r. Crossing positions were obtained by linear interpolation between adjacent wall nodes without smoothing. Crossings within $x/c < 0.02$ were excluded to avoid stagnation-region sign reversals, and crossings beyond $x/c > 0.985$were excluded to avoid trailing-edge artefacts. The upper surface was analysed for positive incidence angles, the lower surface for negative incidence angles, and both surfaces for $\alpha = 0°$. A candidate reattachment was accepted only if it was not followed by another separation within $0.05c$. Shorter reattachment–separation excursions were flagged rather than interpreted as independent closed bubbles. This classification remained unchanged when the threshold was varied between $0.03c$ and $0.12c$, since all observed short excursions were $\le 0.029c$. For cases with an accepted reattachment, the laminar separation bubble length was calculated as

$$L_{\mathrm{LSB}} = x_r - x_s. \qquad (11)$$

Cases without an admissible downstream reattachment crossing were classified as without confirmed reattachment, and no artificial bubble length was assigned.

2.6. Numerical consistency and statistical assessment

The symmetry of the NACA 0012 airfoil was used as an internal check on the combined numerical and post-processing procedure. For matched Tu_∞ and L_s separation and reattachment locations at positive incidence were compared with their mirrored counterparts at the corresponding negative incidence where available. This comparison provides an empirical numerical-consistency reference rather than physical validation or a formal discretization-error estimate. Particular attention was given to x_r, which was more sensitive than $x_s$to the short signed-C_f excursions described above; flagged cases were retained rather than removed from the database. The statistical analysis tested whether the predicted separation response could be represented more compactly by Tu_{LE}than by the nominal inlet turbulence intensity, Tu_∞. The primary comparison used the same pre-specified natural cubic-spline formulation for both descriptors, applied to their logarithms, with four knots spanning the sampled predictor range. Predictive performance was evaluated using leave-one-$(T, u_\infty L_s)$-group-out cross-validation across the 15 inlet-condition groups. We excluded all observations associated with the held-out inlet condition, preventing related cases from appearing simultaneously in the training and validation sets. For each response, the out-of-group prediction error was quantified by the root-mean-square error,

$$\mathrm{RMSE} = \sqrt{\frac{1}{N}\sum_{i=1}^{N}(x_i - \hat{x}_i)^2}. \qquad (12)$$

The relative predictive gain obtained by replacing $Tu_\infty$with $Tu_{LE}$was defined as

$$G = 1 - \frac{\mathrm{RMSE}_{LE}}{\mathrm{RMSE}_\infty}. \qquad (13)$$

where $G > 0$indicates lower cross-validated prediction error for Tu_{LE}. Uncertainty in G was estimated using 5000 cluster-bootstrap resamples at the $(T, u_\infty L_s)$-group level with a fixed random seed of 2026. Only cases with a reliably defined response were included in each response-specific analysis; thus, cases without confirmed reattachment remained eligible for x_s analysis but were excluded when x_r was required. Robustness to statistical model form was assessed using linear, quadratic, natural-spline, and isotonic formulations. Additional comparisons examined whether including L_s alongside Tu_{LE} reduced cross-validated error and whether the resulting residuals retained systematic dependence on the prescribed length scale. These tests were used to assess the relative predictive organization of Tu_∞ and Tu_{LE} within the present steady Transition SST database, without implying that the prescribed turbulence length scale is physically irrelevant.

3. Results and Discussion

3.1. Numerical consistency and external assessment

The near-wall resolution remained within the intended low-y^+ range throughout the investigated cases. Across all 105 cases, the maximum wall coordinate on the Fine grid was $y^+_{\max} = 0.93$, occurring

near the leading edge at $\alpha = 8°$; the median of the case-wise maxima was 0.75. These values support direct resolution of the near-wall region required by the Transition SST formulation. We further assessed numerical consistency using the geometric symmetry of the NACA 0012 airfoil. For matched inlet conditions, we compared separation locations extracted from the upper surface at positive incidence with their lower-surface counterparts at the corresponding negative incidence. The median difference in x_s/c was 0.0035, with a maximum of 0.0067. Reattachment differed by at most $0.004c$ at $\pm 2°$ and $0.008c$ among unflagged cases at $\pm 4°$; differences of up to $0.023c$ occurred only in flagged cases. These differences provide an internal consistency scale for interpreting smaller variations among turbulence-condition cases. The predicted separation topology was externally assessed at $\alpha = 4°$ and 6°, where high-fidelity reference data are available (Fig. 2; Table 2) , with the corresponding reference conditions summarized in Table S5.

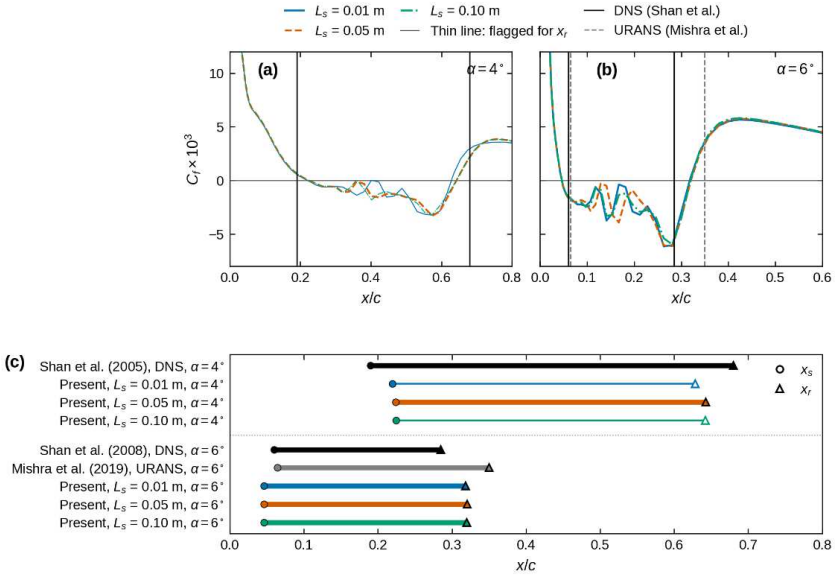


Fig. 2. External assessment of separation topology at $Re_c = 10^5$ and $Tu_\infty = 0.15\%$: signed C_f at **(a)** 4° and **(b)** 6° and **(c)** comparison of extracted separation and reattachment locations with DNS data from Shan et al. (2005, 2008).

Thus, the calculations again reproduce the closed-bubble topology, although quantitative offsets remain in both bubble boundaries. These comparisons provide an external assessment of the predicted topology rather than validating the turbulence parameterization developed below.

Table 2. External assessment of predicted separation and reattachment locations against available high-fidelity results.

Source	α	x_s/c	x_r/c	L_{LSB}/c
Present Transition SST	4°	0.219-0.226	0.623-0.643	0.397-0.419
Shan et al. (2005)	4°	0.19	0.68	≈ 0.49
Present Transition SST	6°	≈ 0.046	0.318-0.321	0.272-0.274
Shan et al. (2008)	6°	0.060	0.285	0.225

Mishra et al. (2019)	6°	0.064	0.350	0.286

3.2. Evolution of turbulence toward the leading edge

The turbulence intensity reaching the leading-edge region differed systematically from the nominal inlet value and depended on the prescribed turbulence length scale. Figure 3 shows Tu_{LE} as a function of Tu_{∞} for the three prescribed length scales. At a fixed Tu_{∞}, different values of L_s produced distinct turbulence levels at the sampling station, demonstrating that identical nominal turbulence intensities do not necessarily represent identical modeled turbulence states approaching the airfoil.

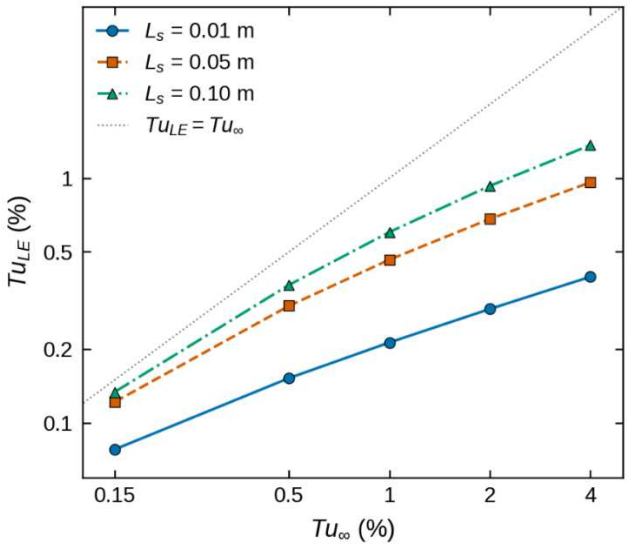


Fig. 3. Evolution of leading-edge turbulence intensity Tu_{LE} with nominal inlet turbulence intensity Tu_{∞} for the three prescribed turbulence length scales.

The descriptor itself was stable with respect to the details of its evaluation. Moving the sampling station upstream produced changes below 0.6% (Fig. S1), while its variation with incidence remained small for a fixed inlet condition (Fig. S2). The local velocity at the sampling point remained within 0.961–0.972 U_{∞} for all cases (Table S1), so normalization by the local rather than the reference velocity would rescale Tu_{LE} almost uniformly. The corresponding case-level values are provided in Table S1.

3.3. Reorganization of the separation response and predictive performance

The effect of replacing the nominal inlet turbulence intensity with the turbulence state reaching the leading-edge region is shown in Fig. 4. When the separation location is plotted against Tu_{∞}, the predicted values retain a systematic spread among the three prescribed turbulence length scales, L_s, and this spread becomes more pronounced as the inlet turbulence level increases [Fig. 4(a, c, e)]. Replotting the same cases against Tu_{LE} produces a noticeably more compact relationship across the tested incidence conditions [Fig. 4(b, d, f)].

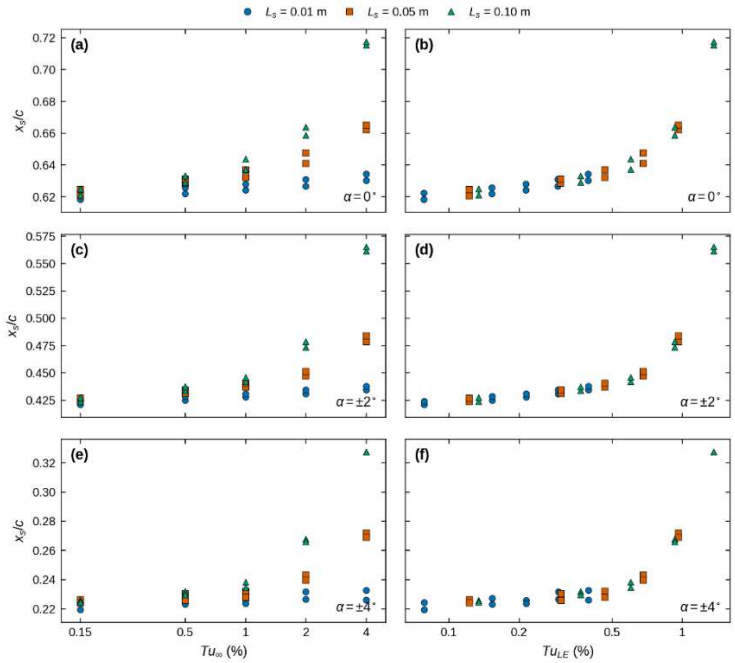


Fig. 4. Reorganization of the predicted separation location using nominal and leading-edge turbulence intensity. Left column: x_s/cplotted against Tu_∞. Right column: the corresponding results plotted against Tu_{LE}. Symbols distinguish the three prescribed turbulence length scales.

Although the collapse is not perfect, much of the systematic L_s-dependent spread present under the nominal inlet specification is reduced when the turbulence descriptor is evaluated immediately upstream of the leading edge. The out-of-group predictive analysis supports the visual reorganization, as summarized graphically in Fig. 5 and quantitatively in Table 3. Across the separation cases, the leading-edge descriptor consistently produced lower prediction error than the nominal inlet turbulence intensity, indicating that it provides a more compact representation of the separation response across the tested inlet conditions.

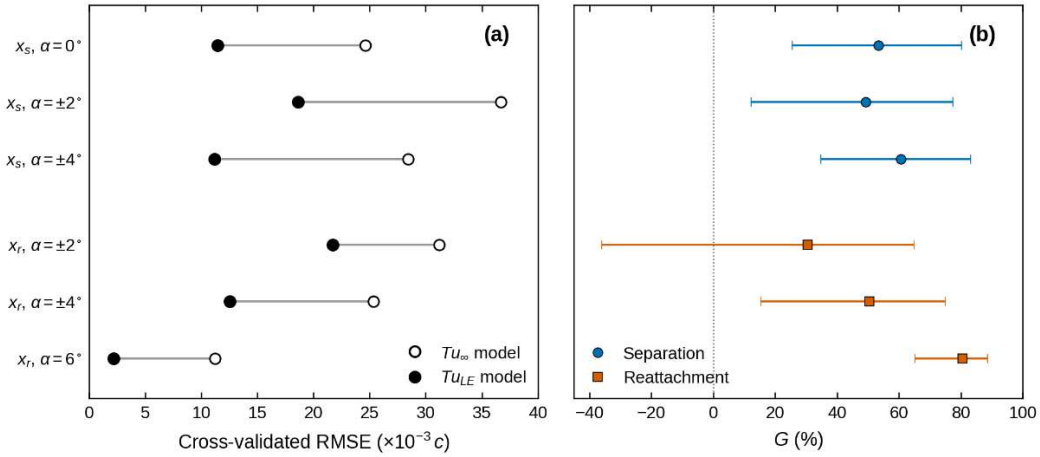


Fig. 5. Out-of-group predictive performance of the Tu_∞- and Tu_{LE}-based models: (a) cross-validated RMSE for separation and reattachment; (b) predictive gain, G, with error bars denoting the cluster-bootstrap confidence intervals. The vertical line at $G = 0$ denotes no predictive improvement.

The same overall tendency was observed for reattachment, although the improvement was less uniform across the incidence groups. The strongest enhancement occurred where reattachment was well defined, whereas the benefit became less consistent in the group exhibiting greater variability.

Table 3. Cross-validated predictive performance using nominal Tu_∞ and leading-edge Tu_{LE}.

Response	Incidence	RMSE, Tu_∞	RMSE, Tu_{LE}	Predictive gain, G	95% CI for G
Separation, x_s/c	0°	0.0246	0.0115	53.4%	25.5 to 80.2%
Separation, x_s/c	±2°	0.0367	0.0186	49.3%	12.3 to 77.4%
Separation, x_s/c	±4°	0.0284	0.0112	60.7%	34.8 to 83.2%
Reattachment, x_r/c	±2°	0.0312	0.0217	30.5%	−35.9 to 64.9%
Reattachment, x_r/c	±4°	0.0253	0.0126	50.4%	15.3 to 75.0%
Reattachment, x_r/c	6°	0.0112	0.00219	80.5%	65.3 to 88.6%

For separation, the confidence intervals remained entirely on the side indicating a predictive advantage for Tu_{LE} across all evaluated incidence groups, supporting a consistent improvement in out-of-group prediction. For reattachment, the uncertainty was more heterogeneous: some incidence groups showed a clearly resolved improvement, whereas one group retained a confidence interval spanning both sides of zero. Accordingly, Tu_{LE} provides a consistently stronger out-of-group descriptor of the predicted separation location than nominal Tu_∞. Its predictive advantage for reattachment is condition dependent.

3.4. Residual length-scale dependence and statistical robustness

The improvement obtained with Tu_{LE} is also reflected in the residual structure. When separation is represented using Tu_∞, mean residuals retain systematic ordering with prescribed L_s (Fig. 6). This systematic ordering is markedly reduced after the response is parameterized by Tu_{LE}, although small residual offsets remain (Fig. 6; Table S4). A stronger test is obtained by retaining L_s explicitly in the predictive models. Adding L_s to the Tu_{LE}-based models increased the cross-validated RMSE in all 18 evaluated response–model combinations (Fig. S5; Table S2), with increases of approximately 0.4–$2.5 \times 10^{-3}c$. Within the present database, prescribed L_s therefore provides no additional out-of-group predictive benefit once Tu_{LE} is included. This result concerns predictive information within the investigated Transition SST framework and does not imply that turbulence length scale is physically irrelevant.

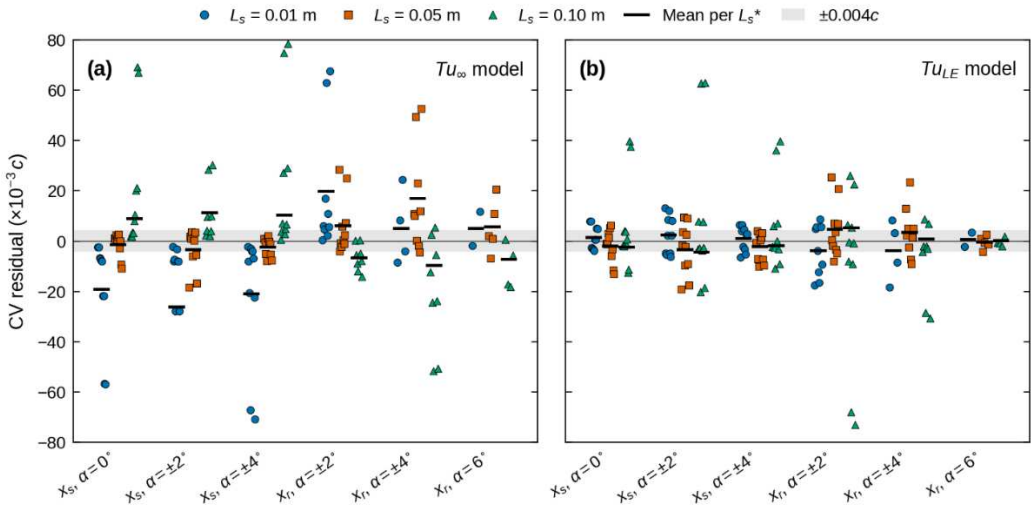


Fig. 6. Mean residual dependence on prescribed turbulence length scale after representing the separation response using Tu_∞ and Tu_{LE}.

The conclusion was also tested against statistical model form. Linear, quadratic, natural-cubic-spline, and isotonic representations produced different magnitudes of predictive gain, but G remained positive in all 24 evaluated response–model combinations (Fig. 7), with a minimum gain of 4.0%. Bootstrap uncertainty for the primary pre-specified spline model is reported separately in Fig. S6 and Table S3. Together, these tests show that the improvement associated with Tu_{LE} is not a consequence of a single selected regression form. The magnitude of the improvement is model dependent, but its direction is robust across the evaluated formulations.

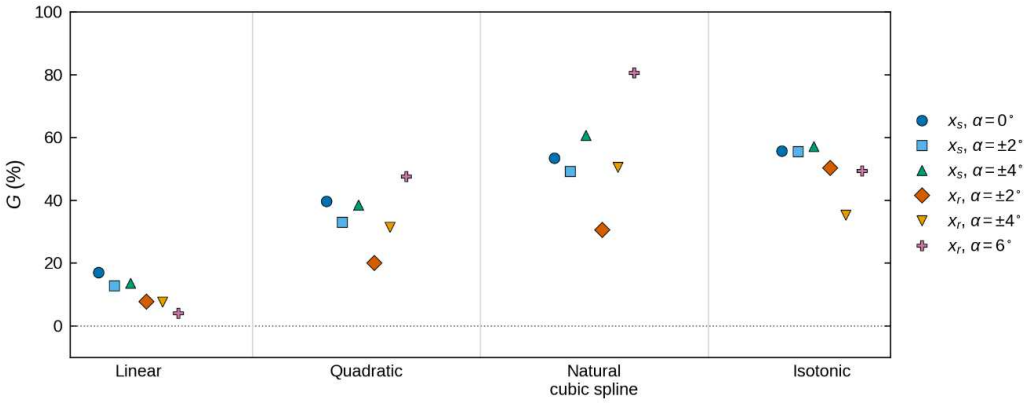


Fig. 7. Sensitivity of predictive gain G to statistical model form. Positive values indicate lower out-of-group prediction error using Tu_{LE} than using Tu_∞.

3.5. Separation versus reattachment

The results reveal a clear distinction between separation and reattachment. For x_s, replacing Tu_∞ with Tu_{LE} reduced cross-validated error across all three evaluated incidence groups, with gains of 49.3–60.7% and confidence intervals entirely above zero. For x_r, the improvement was condition dependent, particularly at

$\pm 2°$, where the confidence interval included zero. The observed-versus-predicted results and residual patterns show the same distinction (Figs. S7 and S8). The signed-C_f diagnostics further demonstrate the greater topological sensitivity of reattachment extraction. Figure 8 illustrates the three outcomes encountered in the automated procedure: an accepted reattachment crossing, a candidate reattachment flagged because of subsequent zero crossings and renewed reversed flow, and a case in which no reattachment was detected upstream of the $x/c = 0.985$exclusion limit.

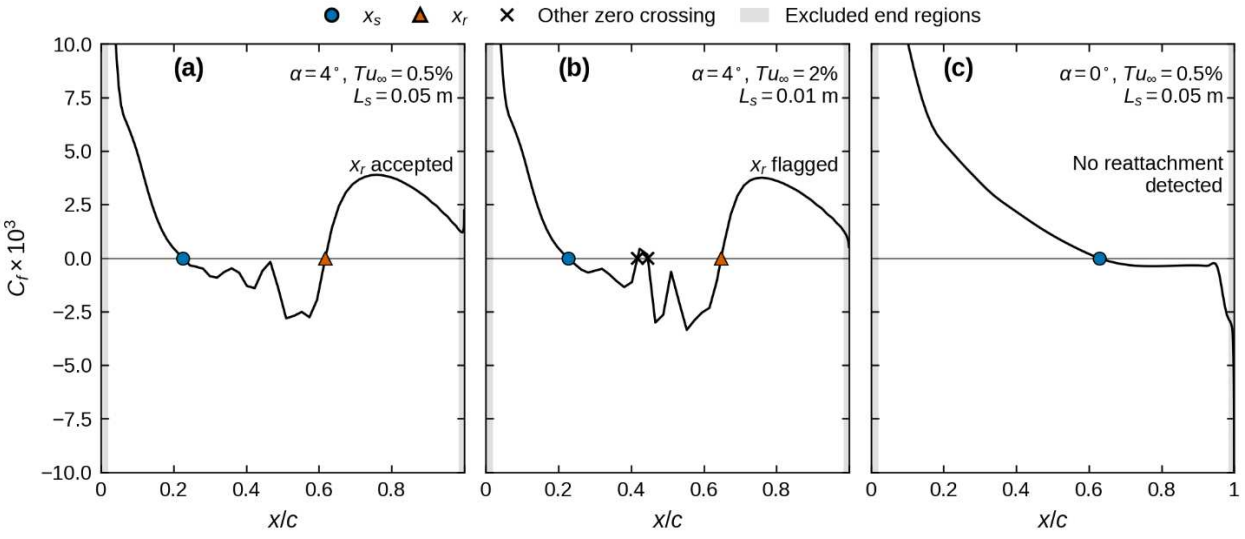


Fig. 8. Representative signed skin-friction coefficient C_f distributions illustrating the reattachment-classification procedure: (a) accepted x_r, (b) x_r flagged because the candidate crossing is followed by additional zero crossings and renewed negative C_f, and (c) no reattachment detected upstream of $x/c = 0.985$. Blue circles denote the extracted separation location x_s, orange triangles denote candidate reattachment locations x_r, crosses indicate other zero crossings, and shaded regions indicate the excluded end regions.

Twenty-five of the 105 suction-side solutions contained short positive-C_f segments followed by renewed separation and were therefore flagged for $x_r$analysis (Table S6). Representative examples of accepted, flagged, and no-reattachment cases are shown in Fig. S3. The number of flagged cases remained unchanged over the tested excursion-threshold range, including the adopted 0.05c criterion (Fig. S4). This threshold sensitivity test indicates that the flagged classification is not an artifact of the particular $0.05c$value selected for the analysis. Reattachment at 8° was not included in the quantitative predictive comparison because 11 of the 15 cases were flagged under this criterion (Table S6). Overall, Tu_{LE}provides the most consistent improvement for prediction of the separation location. Its advantage for reattachment is evident at some incidences but less uniform, consistent with the greater sensitivity of $x_r$to downstream wall-shear topology and separated-flow development.

4. Conclusions and Limitations

The present study examined whether nominal freestream turbulence intensity adequately characterizes the predicted laminar-separation response of a NACA 0012 airfoil at $Re_c = 10^5$, or whether the turbulence state reaching the leading-edge region provides a more informative descriptor. Across the

105-case steady two-dimensional Transition SST database, the reference-normalized leading-edge turbulence intensity, Tu_{LE}, provided a more compact description of the predicted separation response than nominal Tu_{∞}. Replacing Tu_{∞} with Tu_{LE} reduced the out-of-group prediction error for separation location by approximately 49–61% under the pre-specified statistical model, with the corresponding 95% cluster-bootstrap confidence intervals remaining above zero for all three separation groups. The predictive gain also remained positive across all tested statistical formulations. In contrast, the improvement for reattachment location was condition dependent, consistent with its greater sensitivity to downstream separated-flow development and wall-shear topology. The results further indicate that the apparent influence of the prescribed turbulence length scale, L_s, is largely associated with its effect on the modeled upstream turbulence evolution. Conditioning the response on Tu_{LE} reduced the systematic L_s-dependent residual structure, while explicitly adding L_s to the Tu_{LE}-based models increased the cross-validated RMSE in all 18 evaluated response–model combinations. Thus, we detected no additional predictive benefit from prescribed L_s once the turbulence state reaching the leading-edge region was represented in the present calculations. This finding should not be interpreted as evidence that turbulence length scale is physically irrelevant. External comparison with high-fidelity results at 4° and 6° recovered the general closed-bubble topology. However, quantitative differences remained in the predicted separation and reattachment boundaries. The available reference cases do not systematically vary Tu_{∞} and L_s; consequently, they provide an external assessment of the predicted separation topology rather than independent validation of the Tu_{LE} parameterization.

The conclusions are restricted to the NACA 0012 airfoil at $Re_c = 10^5$, the investigated incidence and turbulence ranges, and the steady two-dimensional Transition SST formulation. The calculations do not resolve the three-dimensional and unsteady dynamics of transitional separated shear layers. Furthermore, because freestream disturbances enter the correlation-based Transition SST formulation predominantly through turbulence-intensity-related quantities, the improved organization obtained with Tu_{LE} should be interpreted within the structure of this closure. Physical turbulence length scale may influence transition through disturbance spectra, receptivity, and other mechanisms not explicitly represented in the present model. Within these limits, nominal Tu_{∞} alone does not uniquely characterize the modeled turbulence state reaching the airfoil. For the present calculations, Tu_{LE} is a more effective descriptor of predicted separation location, whereas its advantage for reattachment is less uniform. Accordingly, reporting the turbulence intensity reaching the leading-edge region alongside the prescribed inlet conditions may provide a more informative characterization of transitional RANS calculations. Whether this organization persists at other Reynolds numbers, for other geometries, or in physical and scale-resolving flows requires independent assessment.

Funding

No funding was received for conducting this study or for the preparation of this manuscript.

Competing Interests

The authors declare no relevant financial or non-financial interests to disclose.

Author Contributions

Montaser Ali Saeed: Conceptualization, methodology, numerical investigation, data curation, formal analysis, statistical analysis, visualization, interpretation of results, and writing—original draft.

Alnazir KH. Alatta: Numerical analysis, ANSYS support, and manuscript review.

Saad Adam: Supervision and review of the manuscript.

Abdelgader Agilah Saleh Gheidan: Supervision and review of the manuscript.

All authors reviewed and approved the final manuscript.

Data Availability

The data generated and analyzed during the current study are available from the corresponding author upon reasonable request.

References

Abu-Ghannam, B. J., & Shaw, R. (1980). Natural transition of boundary layers—the effects of turbulence, pressure gradient and flow history. *Journal of Mechanical Engineering Science, 22*, 213–228. https://doi.org/10.1243/JMES_JOUR_1980_022_043_02

Alam, M., & Sandham, N. D. (2000). Direct numerical simulation of 'short' laminar separation bubbles with turbulent reattachment. *Journal of Fluid Mechanics, 410*, 1–28. https://doi.org/10.1017/S0022112099008976

Balzer, W., & Fasel, H. F. (2016). The effect of free-stream turbulence on boundary-layer transition and separation. *Journal of Fluid Mechanics, 801*, 289–321. https://doi.org/10.1017/jfm.2016.424

Boutilier, M. S. H., & Yarusevych, S. (2012a). Parametric study of separation and transition characteristics over an airfoil at low Reynolds numbers. *Experiments in Fluids, 52*, 1491–1506. https://doi.org/10.1007/s00348-012-1270-z

Boutilier, M. S. H., & Yarusevych, S. (2012b). Separated shear layer transition over an airfoil at a low Reynolds number. *Physics of Fluids, 24*, 084105. https://doi.org/10.1063/1.4744989

Breuer, M. (2018). Effect of inflow turbulence on an airfoil flow with laminar separation bubble: An LES study. *Flow, Turbulence and Combustion, 101*, 433–456. https://doi.org/10.1007/s10494-017-9890-2

Gaster, M. (1967). *The Structure and Behaviour of Laminar Separation Bubbles*. Aeronautical Research Council Reports and Memoranda No. 3595.

Hain, R., Kähler, C. J., & Radespiel, R. (2009). Dynamics of laminar separation bubbles at low-Reynolds-number aerofoils. *Journal of Fluid Mechanics, 630*, 129–153. https://doi.org/10.1017/S0022112009006661

Hosseinverdi, S., & Fasel, H. F. (2019). Numerical investigation of laminar–turbulent transition in laminar separation bubbles: The effect of free-stream turbulence. *Journal of Fluid Mechanics, 858*, 714–759. https://doi.org/10.1017/jfm.2018.809

Hrynuk, J. T., Olson, D., Stutz, C. M., & Jackson, J. (2024). Effects of turbulence on NACA 0012 airfoil performance at low Reynolds number. *AIAA Journal, 62*(1), 409–417. https://doi.org/10.2514/1.J063244

Huang, R. F., & Lee, H. W. (1999). Effects of freestream turbulence on wing-surface flow and aerodynamic performance. *Journal of Aircraft, 36*(6), 965–972. https://doi.org/10.2514/2.2537

Istvan, M. S., Kurelek, J. W., & Yarusevych, S. (2018). Turbulence intensity effects on laminar separation bubbles formed over an airfoil. *AIAA Journal, 56*(4), 1335–1347. https://doi.org/10.2514/1.J056453

Istvan, M. S., & Yarusevych, S. (2018). Effects of free-stream turbulence intensity on transition in a laminar separation bubble formed over an airfoil. *Experiments in Fluids, 59*, 52. https://doi.org/10.1007/s00348-018-2511-6

Jardin, T., Ferrand, V., & Gowree, E. R. (2025). NACA0012 airfoil at Reynolds numbers between 50,000 and 140,000—Part 1: Steady freestream. *International Journal of Heat and Fluid Flow, 112*, 109655. https://doi.org/10.1016/j.ijheatfluidflow.2024.109655

Jaroslawski, T., et al. (2023). Disturbance growth in a laminar separation bubble subjected to free-stream turbulence. *Journal of Fluid Mechanics, 956*, A33. https://doi.org/10.1017/jfm.2023.23

Jonáš, P., Mazur, O., & Uruba, V. (2000). On the receptivity of the bypass transition to the length scale of the outer-stream turbulence. *European Journal of Mechanics B/Fluids, 19*(5), 707–722. https://doi.org/10.1016/S0997-7546(00)01094-3

Jones, L. E., Sandberg, R. D., & Sandham, N. D. (2010). Stability and receptivity characteristics of a laminar separation bubble on an aerofoil. *Journal of Fluid Mechanics, 648*, 257–296. https://doi.org/10.1017/S0022112009993089

Kawai, S., Asada, T., & Fujii, K. (2023). Freestream turbulence effects in large-eddy simulations of laminar separation bubble. *Journal of Aircraft, 60*(5), 1721–1727. https://doi.org/10.2514/1.C037058

Kurelek, J. W., Boutilier, M. S. H., & Yarusevych, S. (2016). Coherent structures in a separated flow over a NACA 0018 airfoil. *AIAA Journal, 54*(8), 2295–2309. https://doi.org/10.2514/1.J054820

Langtry, R. B., & Menter, F. R. (2009). Correlation-based transition modeling for unstructured parallelized computational fluid dynamics codes. *AIAA Journal, 47*(12), 2894–2906. https://doi.org/10.2514/1.42362

Lissaman, P. B. S. (1983). Low-Reynolds-number airfoils. *Annual Review of Fluid Mechanics, 15*, 223–239. https://doi.org/10.1146/annurev.fl.15.010183.001255

Malkiel, E., & Mayle, R. E. (1996). Transition in a separation bubble. *Journal of Turbomachinery, 118*, 752–759.

McAuliffe, B. R., & Yaras, M. I. (2010). Transition mechanisms in separation bubbles under low- and elevated-freestream turbulence. *Journal of Turbomachinery, 132*, 011004. https://doi.org/10.1115/1.2812949

Menter, F. R., Langtry, R. B., & Völker, S. (2006). Transition modelling for general purpose CFD codes. *Flow, Turbulence and Combustion, 77*, 277–303. https://doi.org/10.1007/s10494-006-9047-1

Mohamed Aniffa, M., Yarusevych, S., & Boutilier, M. S. H. (2023). Geometry- and pressure-induced laminar separation bubbles subjected to elevated free-stream turbulence. *Journal of Fluid Mechanics, 957*, A19. https://doi.org/10.1017/jfm.2023.53

Mueller, T. J., & DeLaurier, J. D. (2003). Aerodynamics of small vehicles. *Annual Review of Fluid Mechanics, 35*, 89–111. https://doi.org/10.1146/annurev.fluid.35.101101.161102

O'Meara, M. M., & Mueller, T. J. (1987). Laminar separation bubble characteristics on an airfoil at low Reynolds numbers. *AIAA Journal, 25*(8), 1033–1041. https://doi.org/10.2514/3.9739

Olson, D., Katz, J., & Hrynuk, J. T. (2013). On the challenges in experimental characterization of flow separation over airfoils at low Reynolds number. *Experiments in Fluids, 54*, 1470. https://doi.org/10.1007/s00348-013-1470-1

Saric, W. S., Reed, H. L., & Kerschen, E. J. (2002). Boundary-layer receptivity to freestream disturbances. *Annual Review of Fluid Mechanics, 34*, 291–319. https://doi.org/10.1146/annurev.fluid.34.082701.161921

Tani, I. (1964). Low-speed flows involving bubble separations. *Progress in Aerospace Sciences, 5*, 70–103. https://doi.org/10.1016/0376-0421(64)90004-1

Thompson, A., Neunaber, S. P., Hölling, M., & Peinke, J. (2023). Effects of integral length scale variations on the stall characteristics of a wing at high free-stream turbulence conditions. *Journal of Fluid Mechanics, 974*, A9. https://doi.org/10.1017/jfm.2023.789

Toppings, C., & Yarusevych, S. (2025). Low-Reynolds-number aerofoil boundary layer transition in large-scale free stream turbulence. *Journal of Fluid Mechanics, 1021*, A46. https://doi.org/10.1017/jfm.2025.10747

Wang, S., Zhou, Y., Alam, M. M., & Yang, H. (2014). Turbulent intensity and Reynolds number effects on an airfoil at low Reynolds numbers. *Physics of Fluids, 26*, 115107. https://doi.org/10.1063/1.4901969

Yarusevych, S., Sullivan, P. E., & Kawall, J. G. (2009). On vortex shedding from an airfoil in low-Reynolds-number flows. *Journal of Fluid Mechanics, 632*, 245–271. https://doi.org/10.1017/S0022112009007058

Yu, M., Hrynuk, J. T., Booth, D. T., & Poudel, N. (2024). Freestream turbulence effects on low Reynolds number NACA 0012 airfoil laminar separation bubble and lift generation. *Aerospace Science and Technology, 149*, 109145. https://doi.org/10.1016/j.ast.2024.109145

Shan H, Jiang L, Liu C (2005) Direct numerical simulation of flow separation around a NACA 0012 airfoil. Computers & Fluids 34:1096–1114. https://doi.org/10.1016/j.compfluid.2004.09.003

Shan H, Jiang L, Liu C, Love M, Maines B (2008) Numerical study of passive and active flow separation control over a NACA0012 airfoil. Computers & Fluids 37:975–992.

Mishra A, Kumar G, De A (2019) Prediction of separation induced transition on thick airfoil using non-linear URANS based turbulence model. Journal of Mechanical Science and Technology 33:2169–2180. https://doi.org/10.1007/s12206-019-0419-6

Supplementary Files

This is a list of supplementary files associated with this preprint. Click to download.

- SupplementaryTablesS1S6.xlsx